On the Capacitance–Voltage Modeling of Strained Quantum-Well MODFET's

José Eduardo Manzoli, Murilo Araujo Romero, and Oscar Hipólito

***Abstract*— A theoretical model for the capacitance–voltage characteristics of strained modulation-doped field-effect transistors (MODFET's) is developed, based on a self-consistent solution of the Schrödinger and Poisson equations. We report on the first MODFET *C–V* simulator in which the proposed Hamiltonian takes into account the strain caused by lattice mismatch, as well as the position-dependent lattice constant and electron effective mass. It is demonstrated that the inclusion of strain-related energy terms is essential to achieve good agreement between theory and experimental data for the *C–V* characteristics of pseudomorphic-channel devices at high gate voltages. The model is also shown to be a useful tool to predict important device characteristics such as the transconductance.**

***Index Terms*— MODFET's, quantum effect semiconductor devices, quantum-well devices, semiconductor device modeling, semiconductor devices, semiconductor heterojunctions, transistors.**

I. Introduction

MODULATION-DOPED superlattices were proposed by Esaki and Tsu in 1969 [1], but demonstrated only in 1978 [2], after the introduction of the molecular beam epitaxy (MBE) growth technique. In the modulation-doped scheme, the conducting electrons are spatially separated from the ionized donors and confined to a two-dimensional gas, presenting better transport properties (low-field mobility and saturation velocity) when compared to free electrons in bulk semiconductors.

It was soon recognized that these improved transport properties could offer extremely high speed and excellent noise performance in microwave transistors. The first of such devices was demonstrated by a Fujitsu research team in 1980 [3]. Since then, the modulation-doped field-effect transistors (MODFET's) have shown high-frequency performance superior to those of any other microwave or millimeter-wave device. Results already published in the literature include power amplification up to 600 GHz [4] as well as the lowest noise figure ever reported at room temperature [5].

The earliest MODFET's were based on the AlGaAs–GaAs material system. However, by the mid-1980's [6], it was experimentally shown that GaAs-based MODFET's with a pseudomorphic InGaAs channel (indium content ranging from 15 to 25%) were able to yield improved microwave characteristics, due to better carrier confinement. Thus, the next logical step was to employ the InAlAs–InGaAs material system [7], where the In mole fraction in the channel was kept at 53% in order to allow for lattice-matching to the underlying InP substrate. Generally, increasing the In content in the channel leads to reduced electron effective mass, higher conduction band offset, subband separation and ground state occupation, leading to improved device performance. Indeed, strained devices reaching 80% of indium content have been intensively investigated, yielding the highest values of current gain cutoff frequency f_T, up to 340 GHz [8].

The design of pseudomorphic devices is generally based on some empirical guidelines. Thin quantum wells (<100 Å) are required to limit occupancy to the ground state, assuring high electron mobility. Also, the spacer layer thickness is kept around 40 Å to achieve the lowest 2-DEG sheet resistance. Recent designs try to account for the effect of strain by limiting the potential discontinuities in the energy band diagram to about two thirds of the values for the same composition, but without strain.

However, in order to optimize the performance of these strained MODFET's, an accurate and more comprehensive capacitance–voltage charge control model for the heterojunction is needed. Unfortunately, the technical literature shows that very little attention has been given to the effect of lattice strain on the *C–V* characteristics of those devices. Indeed, in the first MODFET model aiming specifically at pseudomorphic structures, published by Ando and Itoh [9], the presence of an InGaAs channel into the MODFET layer sequence is accounted for only by using previously reported values of bandgap differences and conduction band offsets for AlGaAs–InGaAs and InGaAs–GaAs material systems. The electron effective mass remained unchanged from an unstrained bulk InGaAs layer. More recently, a variational formulation was proposed [10] to model the charge control characteristics of strained MODFET's on InP substrates. The same overall treatment regarding the InGaAs channel was used.

In this paper, a numerical model based on a fully quantum-mechanical solution of the Schrödinger and Poisson equations

Manuscript received April 10, 1998; revised September 3, 1998. This work was supported by Fapesp (São Paulo State Research Foundation), CNPq (Brazilian Research Council), and by the computational resources of the CESUP-UFRGS.

J. E. Manzoli was with the São Carlos Physics Institute, University of São Paulo, São Paulo, Brazil. He is now with the Nuclear Energy Research Institute, IPEN/CNEN, São Paulo, CEP 05508–900, Brazil.

M. A. Romero is with the Electrical Engineering Department, São Carlos Engineering School, University of São Paulo, CEP 13560-250, Brazil.

O. Hipólito was with the São Carlos Physics Institute, University of São Paulo, São Paulo, Brazil. He is now with the Center for Technological Research, University of Mogi das Cruzes, Mogi das Cruzes, São Paulo, CEP 08780–210, Brazil.

Publisher Item Identifier S 0018-9197(98)08676-X.

is developed. In contrast to the previous studies mentioned above, our model explicitly incorporates the effects of strain caused by lattice mismatch into the proposed Hamiltonian. Our model is also able to account for the position-dependent lattice constant and electron effective mass. In the following sections, we will start by describing the model developed. Next, it will be demonstrated that the inclusion of the effects of lattice mismatch is paramount to obtain accurate agreement with experimental *C–V* data for pseudomorphic devices at high gate voltages, solving discrepancies previously reported in the literature. Specifically, it is shown that strain effects cannot be completely accounted for by simply adjusting the potential steps of the energy band diagram. The proposed formulation will also be used as an analysis and optimization tool to predict the transcondutance of a strained MODFET structure.

II. Model Description

The model is based on the effective mass approximation, where the electron wavefunction is taken as the product of a Bloch function and an envelope function, solution of the time-independent Schrödinger equation

$$H\phi_i(x) = E_i\phi_i(x). \tag{1}$$

The proposed Hamiltonian takes the kinetic energy operator from the formalism suggested originally by Einevoll [11] while the effective potential energy (V_{eff}) terms are given by the Luttinger–Kohn formulation [12]. Thus, one gets

$$H = -\frac{\hbar^2}{2a(x)}\frac{d}{dx}\frac{[a(x)]^2}{m^*(x)}\frac{d}{dx}\frac{1}{a(x)} + V_{\text{eff}}(x) \tag{2}$$

where x is taken as the direction perpendicular to the epitaxial layers. Therefore, $m^*(x)$ and $a(x)$ are the position-dependent effective mass and lattice constant in the growth direction. The effective potential V_{eff} is given as the sum of four terms

$$V_{\text{eff}}(x) = V_e(x) + C_1(\varepsilon_{xx} + \varepsilon_{yy} + \varepsilon_{zz}) + V_H(x) + V_{XC}(x) \tag{3}$$

where V_e represents the conduction-band edge potential of the undoped structure, i.e., the band-diagram discontinuities, and V_H is the Hartree term due to the electrostatic potential. For completeness, we have also included an exchange-correlation term V_{XC} by using the analytical parametrization proposed by Hedin and Lundqvist [13]. C_1 is the conduction band deformation potential and ε_{xx}, ε_{yy}, and ε_{zz} are the strain components, which, considering cubic symmetry, are determined by the elastic constants of the pseudomorphic layer [14]. It was assumed that the hydrostatic strain shift of the conduction band edge with respect to the average valence band edge is governed by a deformation potential in the range of -6 to -8 eV [15]. It should be stressed that conventional MODFET *C–V* simulators previously reported in the literature include neither the strain component of the effective potential, the second term on the right-hand side of (3), nor the generalized kinetic energy term used in (2).

The one-dimensional Poisson equation, which yields the above-mentioned Hartree term, is given by

$$\frac{d}{dx}\left(\varepsilon_o\varepsilon_r(x)\frac{d}{dx}\right)V_H(x) = -q[N_D^+(X) - N_A^- - n(x)] \tag{4}$$

where q is the electronic charge, ε_o is the dielectric permittivity in vacumm, $\varepsilon_r(x)$ is the position-dependent dielectric constant of the semiconductor, N_D^+ is the ionized donor concentration, N_A^- is the ionized nonintentional background acceptor concentration, and $n(x)$ is the free-electron concentration in the conduction band (the free hole concentration has been neglected). We write $n(x)$ in terms of the electronic eigenfunction $\phi_i(x)$ as [16]

$$n(x) = \frac{m_o^* kT}{\pi\hbar^2}\sum_t \ln\left[1 + \exp\left(\frac{E_f - E_i}{kT}\right)\right]|\phi_i(x)|^2 \tag{5}$$

where m_o^* is the electron effective mass in the 2-DEG channel, k is the Boltzmann constant, T is the absolute temperature, $\hbar$ is the reduced Planck constant, E_f is the Fermi level energy, and E_i represents the ith eigenvalue. Summation is carried out over all i subbands.

The ionized donor concentration N_D^+ is described by [16]

$$N_D^+(x) = \frac{N_D(x)}{1 + g_n\exp[(E_f - E_d)/kT]} \tag{6}$$

where N_D is the position-dependent donor concentration, g_n is the donor level spin degeneracy factor (taken as equal to 2), and E_D is the donor ionization energy.

The Fermi-level position E_f is computed from the usual charge neutrality condition in the bulk material and the above formulation [see (1)–(6)] must be solved self-consistently in real space. In particular, the eigenstates of the Schrödinger equation are calculated by using a split-operator algorithm (appendix), through a nonuniform finite difference discretization scheme [17], under the boundary conditions that the wavefunction must vanish at the substrate and the Schottky barrier. The boundary conditions for the Poisson equation are given by the applied gate voltage at the Schottky barrier (taken as $x = 0$) as well as by the position of the conduction band with respect to the Fermi level in the bulk semiconductor, presenting a nonintentional background ionized doping density N_A^- [see (4)].

The numerical procedure employed for a single bias point is summarized by the flow chart diagram of Fig. 1. The algorithm is assumed to have achieved convergence when the expected value $\langle X\rangle$ for the position of the higher subband eigenfunction does not change its value by more than 10^{-5} Å during the last ten steps of imaginary time evolution (see the appendix). For each bias point of the pseudomorphic structure described in Section III-A, convergence in capacitance calculations (four subbands taken into account) was achieved in about 35 s of CPU time on a CRAY-YMP2E computer, i.e., in about 2000 steps of self-consistent Poisson–Schrödinger imaginary time evolution.

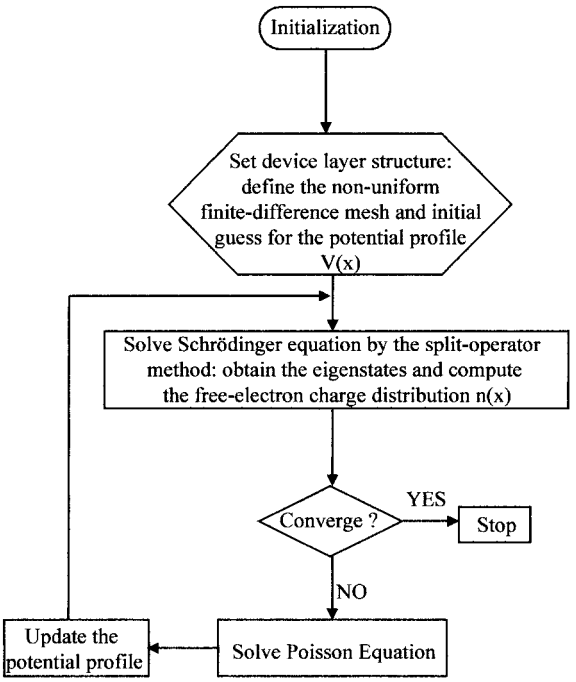

Fig. 1. Flowchart diagram of the self-consistent Schrödinger–Poisson solver.

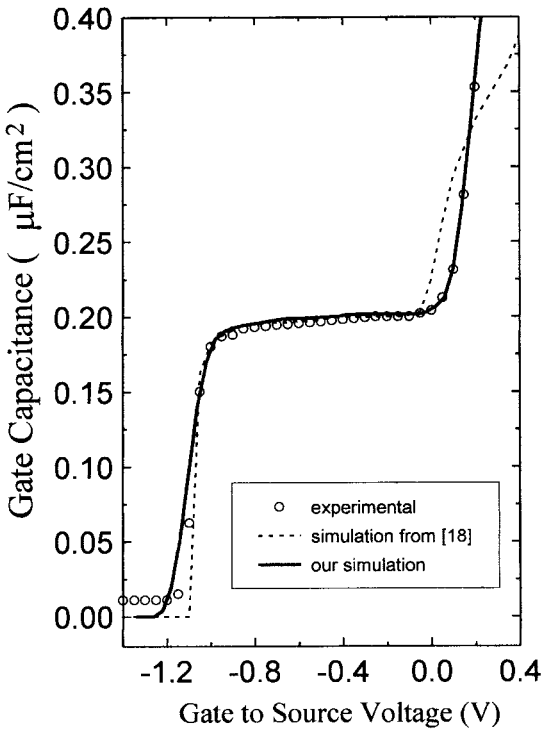

Fig. 2. Experimental and simulated *C–V* curves for an InGaAs channel pseudomorphic MODFET.

III. Results and Discussion

A. Pseudomorphic InGaAs Channel Device

The first structure to be discussed is a conventional AlGaAs–InGaAs pseudomorphic device, fabricated by Eastman's group at Cornell University. The layer structure was given as follows [18]. First, a 1-μm undoped buffer layer is grown on a LEC GaAs substrate, followed by the 170-Å undoped $In_{0.15}Ga_{0.85}As$ pseudomorphic channel and a 25-Å $Al_{0.15}Ga_{0.85}As$ spacer layer. Finally, a 375-Å n^+ donor layer $Al_{0.15}Ga_{0.85}As$ was grown, followed by graded-composition AlGaAs over 100 Å. On top of the graded AlGaAs, 333 Å of n^+ GaAs material is grown to act as a cap layer. FATFET geometries (96 μm$\times$ 96 μm) were used to obtain the experimental MODFET *C–V* profile shown in Fig. 2 [18]. The temperature was kept at 77 K under dark conditions. No further information on the measurement technique was given.

Our theoretical MODFET *C–V* profile was computed by a quasi-static approach, in which the gate capacitance per unit area is given by the total charge variation caused by a small voltage change around a given bias point. In the simulations, the Schottky barrier height was taken as 0.88 eV [9] and the conduction band offsets at the $Al_{0.15}Ga_{0.85}As$–$In_{0.15}Ga_{0.85}As$ and $In_{0.15}Ga_{0.85}As$–GaAs interfaces were assumed to be 0.23 and 0.12 eV, respectively [18]. The donor layer doping was taken to be 10^{18} cm^{-3}. Finally, the residual acceptor density in the GaAs buffer layer was taken as a constant equal to 3.5×10^{15} cm^{-3}. The remaining material parameters are listed in Table I, which concerns the device of Section III-B as well.

Fig. 2 depicts the final numerical results, compared to the experimental and simulated MODFET *C–V* profiles, both presented in [18]. The reason for the discrepancy observed by the Cornell group (dashed lines) at reverse bias voltages smaller than -1.2 V is unclear. It might be due to some modeling assumption regarding the onset of nonzero capacitance. In any case, it is clearly seen that our model (solid lines) yields very good agreement over the whole voltage range of operation. In particular, it correctly predicts the shape of the *C–V* relationship, even for gate voltages above -0.2 V, suggesting that the discrepancy observed by the Cornell group at this voltage region may be caused by changes in the heterostructure effective potential induced by lattice strain, since those effects were not included in their model.

In order to further investigate this hypothesis, we carried out a second numerical simulation using the same device layer sequence and parameters. In Fig. 3, we compute the effects of the lattice strain energy terms [see (2) and (3)] on subband position and electronic density. Regarding the first subband, strain-induced changes are small. However, Fig. 3 clearly indicates that the inclusion of lattice strain in the system Hamiltonian dramatically modifies the results obtained for higher order subbands, supporting the hypothesis stated previously. Indeed, as the gate voltage increases, the higher order subbands become more populated, considerably affecting the device performance and making strain-induced effects much more pronounced in the positive bias regime.

A more detailed inspection of Fig. 3 shows that, for a reverse bias greater than 0.4 V, the inclusion of strain produces no change on the simulation results. In this voltage range, the heterostructure presents no resonances between the electronic subbands. However, it is seen that, as the gate voltage becomes

TABLE I
MATERIAL PARAMETERS USED IN THE SIMULATIONS: m^*, a, ε_r, C_{11} AND C_{12} REPRESENT, RESPECTIVELY, THE ELECTRON EFFECTIVE MASS, THE LATTICE CONSTANT, THE RELATIVE DIELECTRIC CONSTANT, THE DEFORMATION POTENTIAL, AND THE ELASTIC CONSTANTS

	GaAs	InP	$Al_{0.15}Ga_{0.85}As$	$In_{0.15}Ga_{0.85}As$	$In_{0.53}Ga_{0.47}As$	$Al_{0.60}In_{0.40}As$	$Al_{0.48}In_{0.52}As$
m^* [19-20]	$0.067m_o$	$0.08\ m_o$	$0.0794\ m_o$	$0.2\ m_o$	$0.041\ m_o$	$0.15\ m_o$	$0.134\ m_o$
a [19-20]	5.6533 Å	5.8688 Å	5.6533 Å	5.7141 Å	5.8688 Å	5.8153 Å	5.8688 Å
ε_r [19-20]	13.18	12.4	12.7	13.4	13.9	12.52	12.03
C_{11} [19-20]				11.34 (10^{11}dyn/cm^2)		10.54 (10^{11}dyn/cm^2)	
C_{12} [19-20]				5.25 (10^{11}dyn/cm^2)		5.23 (10^{11}dyn/cm^2)	

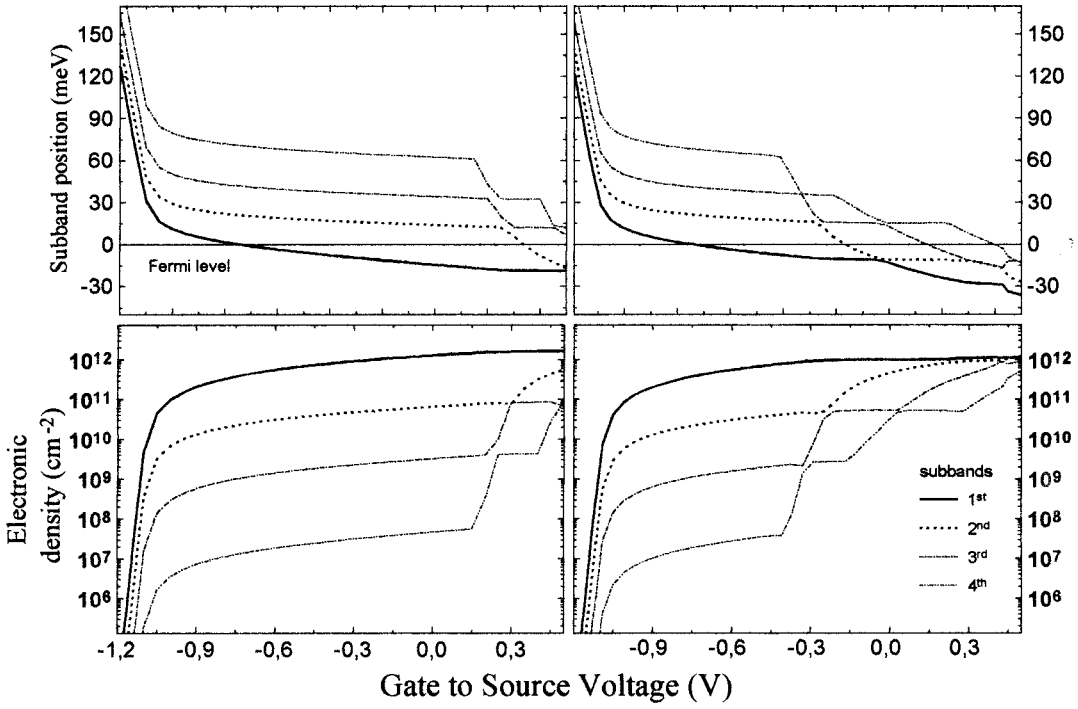

Fig. 3. Subband position and electronic densities as a function of gate bias voltage. Left: no inclusion of strain-induced effects. Right: strain-induced effects accounted for.

more positive, the effect of strain is to enhance the intersubband coupling and to cause a greater number of resonances, changing the shape of the *C–V* relationship.

B. InP-Based Device

In the next step, we investigated an InP based MODFET. The simulated layer sequence on top of the InP substrate is given as follows: a 0.25-μm $Al_{0.48}In_{0.52}As$ buffer layer, the 300-Å Si δ-doped (0.5×10^{18} cm^{-3}) $Ga_{0.47}In_{0.53}As$ quantum well channel, a 15-Å $Al_{0.48}In_{0.52}As$ spacer, a 50-Å n-doped (2.0×10^{18} cm^{-3}) $Al_{0.48}In_{0.52}As$ donor layer and a 225-Å undoped $Al_{0.60}In_{0.40}As$ strained layer. The Schottky barrier height was taken as 0.65 eV and the conduction band offsets at the InP–$Al_{0.48}In_{0.52}As$, $Al_{0.48}In_{0.52}As$–$In_{0.53}Ga_{0.47}As$, and $Al_{0.48}In_{0.52}As$–$Al_{0.60}In_{0.40}As$ interfaces are assumed to be 0.3, 0.55, and 0.2138, respectively. The values were obtained by interpolating Adachi's data [19], [20]. The residual acceptor density in the buffer layer was taken as a constant equal to 10^{15} cm^{-3} and the remaining material parameters are listed in Table I. A sketch of the conduction band potential profile, obtained by using our Schrödinger–Poisson solver at a forward gate bias voltage of 0.35 V, is displayed in Fig. 4.

The goal of the simulation was to check the model capability to predict important device parameters, such as the transconductance g_m, for a fairly complex layer structure. Since our simulation indicates that the depth of the quantum-well channel keeps the electronic concentration in the bulk material negligible up to a forward bias of 0.4 V, we used the velocity saturation approximation for short-channel devices [21] to directly compute the device transconductance

$$g_m = \frac{v_s C_{g,2-\mathrm{DEG}}}{L} \tag{7}$$

where v_s is the electron saturation velocity in the doped 2-DEG channel, taken as 0.7×10^7 cm/s, $C_{g,2-\mathrm{DEG}}$ is the gate

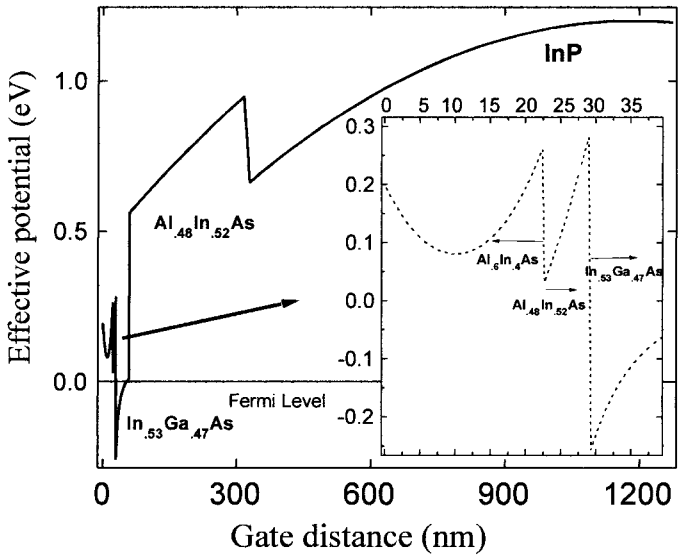

Fig. 4. Self-consistent effective potential profile for a strained InP-based MODFET.

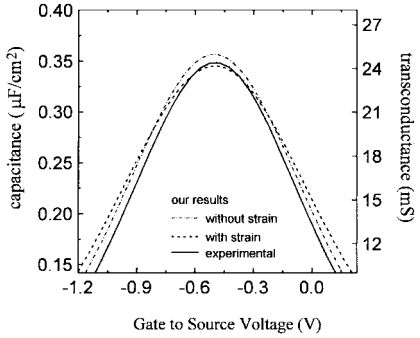

Fig. 5. 2-DEG component of the gate capacitance and corresponding transconductance as a function of gate-to-source voltage for the Hughes MODFET.

capacitance component due to the 2-DEG electrons and L is the gate length. The numerical results were then compared to the experimentally measured characteristics of a InP MODFET fabricated by Hughes Research Labs [22] with 50 μm of gate width and 0.25 μm of gate length. The layer structure below the gate is essentially the same as described in the above paragraph. The only difference is that the top 175-Å of the strained layer consists of $Al_{0.60}In_{0.40}P$ instead of $Al_{0.60}In_{0.40}As$. Given the lack of data on the material parameters for the $Al_{0.60}In_{0.40}P$ alloy, no change was made in the simulated structure.

Fig. 5 displays the results for the device transconductance as a function of gate-to-source voltage. First, it should be observed that the model yields very close agreement with the experimental characterization performed at our laboratory, demonstrating that our simulator can be a useful modeling and optimization tool for MODFET transistors. Also, one expects that the strain, which occurs outside the 2-DEG channel, should not significantly affect the MODFET transport properties. Indeed, our theoretical results indicate that here,

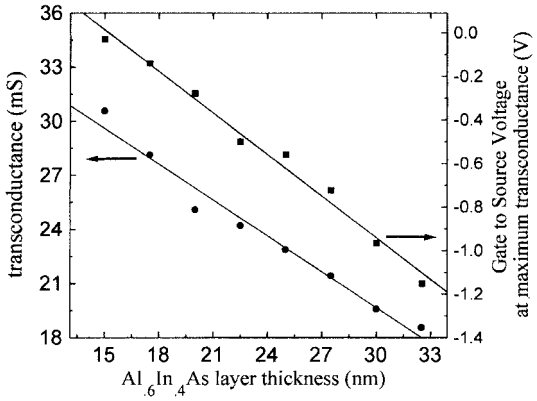

Fig. 6. Peak transconductance and associated gate-to-source voltage as a function of $Al_{0.6}In_{0.4}As$ layer thickness.

in contrast to the case of the previous section, strain effects play a small role on the device performance, causing only a degradation of about 3% on the transconductance peak value.

Further clarification is provided in Fig. 6. In this simulation, we studied the influence of the strained layer thickness on the transconductance peak value, as well as on the gate-to-source voltage for which this maximum value occurs. Although Fig. 6 shows that both parameters can be widely tailored, the strain degradation on the transconductance peak value remained around 4 to 3%, as the strained layer thickness is varied from 325 down to 150 Å.

IV. Conclusion

A self-consistent model for the capacitance-voltage characteristics of strained MODFET's was reported. For the first time in the literature, the proposed C-V simulator includes the lattice-strain energy terms directly into the Hamiltonian. It is demonstrated that strain related effects must be accounted for in order to properly understand the relationship between capacitance and gate to source voltage for strained quantum-well channel MODFET's at forward gate biases. On the contrary, in pseudomorphic devices where the strain is placed away from the 2-DEG channel, no relevant performance changes were observed. The model is shown to a be useful prediction and tailoring tool for important MODFET parameters such as the transconductance.

Appendix

The technique used to obtain the eigenvalues of the Hamiltonian described by (2) and (3) is based on the split operator scheme [23], used previously by the authors to model the time evolution of a wave packet on a proposed finite-superlattice submillimeter-wave emitter [24]. The method starts from the solution of the time-dependent Schrödinger equation for a slowly varying Hamiltonian, formally given by

$$\Psi(t+\Delta t) = e^{\frac{1}{i\hbar}\int_t^{t+\Delta t} H dt}\Psi(t) \cong e^{-iH\Delta t/\hbar}\Psi(t). \quad \text{(A1)}$$

Then, the time evolution of the wave packet Ψ is obtained according to the procedure described by Degani [23]. The

Hamiltonian is split into a kinetic operator (K) and a potential operator (V)

$$\begin{aligned} e^{-iH\Delta t/\hbar} &= e^{\frac{-i\Delta t}{\hbar}[K+V]} = e^{\frac{-i\Delta t}{\hbar}[V/2+K+V/2]} \\ &\cong e^{\frac{-i\Delta t}{\hbar}(V/2)} e^{\frac{-i\Delta t}{\hbar}K} e^{\frac{-i\Delta t}{\hbar}(V/2)} \\ &= \Gamma_1(x) e^{cK} \Gamma_1(x) \end{aligned} \tag{A2}$$

where Γ_1 and c were used to simplify the mathematical notation. Due to the noncomutativity of K and V, this is an approximation of order $(\Delta t)^3$.

In order to propagate the wave function in real space, the exponential is approximated as the unitary operator below

$$e^{cK} \cong \frac{1+cK/2}{1-cK/2} \tag{A3}$$

which has an exact expansion up to the $(\Delta t)^2$ order.

As shown by (A2), in order to obtain the wave packet time evolution, we first operate Γ_1 on Ψ. Then (A3) is applied on the resulting function. Let $\Gamma_1 \Psi = \zeta(x,t)$, so

$$\begin{aligned} \frac{1+cK/2}{1-cK/2}\xi &= \eta \\ (1+cK/2)\xi &= (1-cK/2)\eta. \end{aligned} \tag{A4}$$

Writing (A4) in the finite diference form in a nonuniform mesh [17], the N points in which the function η was discretized, η_i, are the unknown variables of a tridiagonal nonhomogeneous linear system of equations. Once the system is solved and η is calculated, one computes $(C_1\eta)$ and gets the time evolution of Ψ.

The n electronic eigenstates and eigenenergies are easily obtained by propagating a wave packet through the evolution above, now in imaginary time (i.e., the variable t, or Δt, is changed to $-it$). In fact, since any wave function $\Psi(x,t)$ can be expanded in the basis of eigenfunctions of H by

$$\Psi = \sum_j b_j(t)\varphi_j = \sum_j (a_j e^{-iE_j t/\hbar})\varphi_j. \tag{A5}$$

One gets

$$\begin{aligned} \frac{\Psi}{\sqrt{\langle \Psi \mid \Psi \rangle}} &= \frac{\sum_{j=0} a_j e^{-E_j\tau/\hbar}\varphi_j}{\left[\sum_{j=0} |a_j|^2 e^{-2E_j\tau/\hbar}\right]^{1/2}} \\ &= \frac{\frac{a_0}{|a_0|}\varphi_0 + \sum_{j=1} \frac{a_j}{|a_0|} e^{-(E_j-E_0)\tau/\hbar}\varphi_j}{\left[1+\sum_{j=1} \frac{|a_j|^2}{|a_0|^2} e^{-2(E_j-E_0)\tau/\hbar}\right]^{1/2}}. \end{aligned} \tag{A6}$$

Thus, in the limit that $\tau \to \infty$ (which typically means a few hundred steps of imaginary time evolution), the function Ψ becomes the ground state. The extension for higher order eigenstates is then easily accomplished by repeating the algorithm for n linearly independent wave packets and imposing the Gram–Schmidt orthonormalization procedure. Finally, the corresponding j eigenstate associated to each j eigenfunction is given by $\langle \varphi_j | H | \varphi_j \rangle$.

On a final note, we should observe that the temporal step is chosen in such way to assure fast convergence. As a general guideline, we followed a rule which is strictly valid only for linear parabolic partial equations with unitary coefficients and uniform discretization but useful here. It relates the time step and the spatial discretization interval of the finite-difference scheme by $\Delta\tau/(\Delta x_{\min})^2 \leq 0.5$ fs/Å^2.

ACKNOWLEDGMENT

The authors would like to thank J. Brown (Hughes Research Laboratories) for providing the InP MODFET samples.

REFERENCES

[1] L. Esaki and R. Tsu, "Superlattice and negative conductivity in semiconductors," *IBM Res. Rep. RC-2418*, Mar. 1969.
[2] R. Dingle, H. L. Stormer, A. C. Gossard, and W. Wiegmann, "Electron mobilities in modulation-doped semiconductor heterojunction superlattices," *Appl. Phys. Lett.*, vol. 38, no. 10, pp. 665–667, Oct. 1978.
[3] T. Mimura, S. Hyamizu, T. Fujii, and K. Nambu, "A new field-effect transistor with selectively doped GaAs/n-$Al_xGa_{1-x}As$," *Jpn. J. Appl. Phys.*, vol. 19, no. 8, pp. L225–L227, Aug. 1980.
[4] P. M. Smith, S. M. J. Liu, M. Y. Kao, P. Ho, S. C. Wang, K. H. G. Duh, S. T. Fu, and P. C. Chao, "W-band high efficiency InP based power HEMT with 600 GHz $f_{\max}$," *IEEE Microwave Guided Wave Lett.*, vol. 5, pp. 230–232, July 1995.
[5] K. H. G. Duh, P. C. Chao, S. M. J. Liu, P. Ho, M. Y. Kao e, and J. M. Ballingall, "A super low-noise 0.1 μm T-gate InAlAs-InGaAs-InP HEMT," *IEEE Microwave Guided Wave Lett.*, vol. 1, pp. 114–116, May 1991.
[6] T. Henderson, M. I. Aksun, S. K. Peng, H. Morkoç, P. C. Chao, P. M. Smith, K. H. G. Duh, and L. F. Lester, "Microwave performance of a quarter-micrometer gate low-noise pseudomorphic InGaAs/AlGaAs modulation-doped field effect transistor," *IEEE Electron Device Lett.*, vol. 7, pp. 649–651, Dec. 1986.
[7] U. K. Mishra, A. S. Brown, S. E. Rosenbaum, C. E. Hooper, M. W. Pierce, M. J. Delaney, and S. Vaughn, "Microwave performance of AlInAs/GaInAs HEMT's with 0.2 μm and 0.1 μm gate length," *IEEE Electron Device Lett.*, vol. 9, pp. 647–649, Dec. 1988.
[8] L. D. Nguyen, A. S. Brown, M. A. Thompson, and L. M. Jelloian, "50 nm self-aligned gate pseudomorphic AlInAs/GaInAs high-electron mobility transistors," *IEEE Trans. Electron Devices*, vol. 39, pp. 2007–2014, Dec. 1992.
[9] Y. Ando and T. Itoh, "Analysis of charge control in pseudomorphic two-dimensional electron-gas field-effect transistors," *IEEE Trans. Electron Devices*, vol. 35, pp. 2295–2301, Dec. 1988.
[10] G. Halkias, A. Vegiri, G. Pananakakis, and A. Christou, "Efficient charge control model for pseudomorphic and strained high electron mobility transistors on GaAs and InP substrates," *Solid State Electron.*, vol. 35, no. 4, pp. 459–465, Apr. 1992.
[11] G. T. Einevoll, "Operator ordering in effective-mass theory for heterostructures. II. Strained systems," *Phys. Rev. B*, vol. 42, no. 6, pp. 3497–3502, Aug. 1990.
[12] J. M. Luttinger and W. Kohn, "Motion of electrons and holes in perturbed periodic fields," *Phys. Rev.*, vol. 97, no. 4, pp. 869–883, Feb. 1955.
[13] J. H. Oh, K. J. Chang, and G. Ihm, "Electronic structure of $In_{1-x}Ga_x$ As/GaAs strained quantum wells with a δ-doped layer," *J. Phys.: Condensed Matter*, vol. 8, no. 11, pp. 1705–1712, Mar. 1996.
[14] L. Hedin and B. I. Lundqvist, "Explicit local exchange-correlation potential," *J. Phys. C: Solid State Physics*, vol. 4, no. 14, pp. 2064–2083, Oct. 1971.
[15] M. J. Kelly, *Low-Dimensional Semiconductors: Materials, Physics, Technology and Devices*. Oxford, U.K.: Oxford Science, 1995.
[16] S. Wang, *Fundamentals of Semiconductor Theory and Device Physics*. Englewood Cliffs, NJ: Prentice-Hall, 1989.
[17] I. H. Tan, G. L. Snider, L. D. Chang, and E. L. Hu, "A self-consistent solution of Schrödinger and Poisson equations using a nonuniform mesh," *J. Appl. Phys.*, vol. 68, no. 8, pp. 4071–4076, Oct. 1990.
[18] L. D. Nguyen, W. J. Schaff, P. J. Tasker, A. N. Lepore, L. F. Palmateer, M. C. Foisy, and L. F. Eastman, "Charge control, DC and RF performance of a 0.35 μm pseudomorphic AlGaAs/InGaAs modulation-doped field-effect transistor," *IEEE Trans. Electron Devices*, vol. 35, pp. 139–144, Feb. 1988.
[19] S. Adachi, "GaAs, AlAs and $Al_xGa_{1-x}As$: Material parameters for use in research and device applications," *J. Appl. Phys.*, vol. 58, no. 3, pp. R1–R29, Aug. 1985.
[20] S. Adachi, "Material parameters of $In_{1-x}Ga_xAs_yP_{1-y}$ and related binaries," *J. Appl. Phys.*, vol. 53, no. 12, pp. 8775–8792, Dec. 1982.
[21] S. M. Sze, *Physics of Semiconductor Devices*. New York: Wiley, 1981.

[22] J. Brown, Huges Co., personal communication.
[23] M. H. Degani, "Stark ladders in strongly coupled GaAs-AlAs superlattices," *Appl. Phys. Lett.*, vol. 59, no. 1, pp. 57–59, July 1991.
[24] J. E. Manzoli and O. Hipólito, "Numerical simulation of electronic behavior in a finite superlattice with a tamm state: A possible submillimeter wave emitter without optical pumping," in *Proc. Infrared Applications of Semiconductors: Materials, Processing and Devices, Materials Research Society*, Pittsburgh, PA, 1997, vol. 450, pp. 439–444.

José Eduardo Manzoli was born in Araraquara, Brazil, in 1968. He received the B.Sc. degree in physics (with honors) in 1990, the M.Sc. degree in physics in 1993, and the D.Sc. in material sciences and engineering from University of Sao Paulo, Brazil, in 1990, 1993, and 1998, respectively. During his post-graduated program he studied and developed numerical methods for the simulation of semiconductor heterostructures.

He is currently a Researcher in nuclear physics at Instituto de Pesquisas Energéticas e Nucleares (IPEN)—Comissao Nacional de Energia Nuclear (CNEN)—São Paulo, Brazil.

Dr. Manzoli is a member of the Material Research Society (MRS) and of the Brazilian Physics Society (SBF).

Murilo Araujo Romero was born in Rio de Janeiro, Brazil, in 1965. He received the B.Sc. and M.Sc. degrees in electrical engineering from Pontifical Catholic University of Rio de Janeiro, Brazil, in 1988 and 1991, respectively, and the Ph.D. from Drexel University, Philadelphia, PA, in 1995.

Since then, he has been an Assistant Professor of Electrical Engineering at University of São Paulo, São Carlos, Brazil. His current research interests are the modeling and simulation of optoelectronic semiconductor devices and circuits as well as optical fiber sensors.

Oscar Hipólito, photograph and biography not available at the time of publication.